

A meshless algorithm with the improved moving least square approximation for nonlinear improved Boussinesq equation

Yu Tan(谭渝) and Xiao-Lin Li(李小林)

Citation: Chin. Phys. B, 2021, 30 (**1**): 010201. DOI: 10.1088/1674-1056/abaed7
Journal homepage: http://cpb.iphy.ac.cn; http://iopscience.iop.org/cpb

What follows is a list of articles you may be interested in

Improved reproducing kernel particle method for piezoelectric materials

Ji-Chao Ma(马吉超), Gao-Feng Wei(魏高峰), Dan-Dan Liu(刘丹丹)
Chin. Phys. B, 2018, 27 (**1**): 010201. DOI: 10.1088/1674-1056/27/1/010201

Topology optimization using the improved element-free Galerkin method for elasticity

Yi Wu(吴意), Yong-Qi Ma(马永其), Wei Feng(冯伟), Yu-Min Cheng(程玉民)
Chin. Phys. B, 2017, 26 (**8**): 080203. DOI: 10.1088/1674-1056/26/8/080203

Meshless analysis of an improved element-free Galerkin method for linear and nonlinear elliptic problems

Yao-Zong Tang(唐耀宗), Xiao-Lin Li(李小林)
Chin. Phys. B, 2017, 26 (**3**): 030203. DOI: 10.1088/1674-1056/26/3/030203

Two-dimensional fracture analysis of piezoelectric material based on the scaled boundary node method

Shen-Shen Chen(陈莘莘), Juan Wang(王娟), Qing-Hua Li(李庆华)
Chin. Phys. B, 2016, 25 (**4**): 040203. DOI: 10.1088/1674-1056/25/4/040203

Solving unsteady Schrödinger equation using the improved element-free Galerkin method

Rong-Jun Cheng(程荣军) and Yu-Min Cheng(程玉民)
Chin. Phys. B, 2016, 25 (**2**): 020203. DOI: 10.1088/1674-1056/25/2/020203

A meshless algorithm with the improved moving least square approximation for nonlinear improved Boussinesq equation*

Yu Tan(谭渝) and Xiao-Lin Li(李小林)†

School of Mathematical Sciences, Chongqing Normal University, Chongqing 400047, *China*

(Received 8 July 2020; revised manuscript received 26 July 2020; accepted manuscript online 13 August 2020)

An improved moving least square meshless method is developed for the numerical solution of the nonlinear improved Boussinesq equation. After the approximation of temporal derivatives, nonlinear systems of discrete algebraic equations are established and are solved by an iterative algorithm. Convergence of the iterative algorithm is discussed. Shifted and scaled basis functions are incorporated into the method to guarantee convergence and stability of numerical results. Numerical examples are presented to demonstrate the high convergence rate and high computational accuracy of the method.

Keywords: meshless, improved moving least square approximation, nonlinear improved Boussinesq equation, convergence and stability

PACS: 02.60.Cb, 02.60.Lj, 03.65.Ge **DOI:** 10.1088/1674-1056/abaed7

1. Introduction

The nonlinear improved Boussinesq equation[1] is a new form of the famous Boussinesq equation.[2,3] By using u_{xxtt} instead of u_{xxxx}, the improved Boussinesq equation is physically stable and thus effectively overcomes the unrealistic instability of the bad Boussinesq equation. The improved Boussinesq equation can be used to model some physical phenomena such as sound waves,[1] acoustic waves on elastic rods,[4] and plasma waves at right angles to the magnetic field.[5] Over the past four decades, some numerical methods, such as the finite difference method (FDM),[6–9] the finite element method (FEM),[6,10] the finite volume element method (FVEM),[11,12] the Fourier pseudospectral method,[13] the radial basis functions method,[14] the local discontinuous Galerkin (LDG) method,[15] and the multisymplectic method,[16] have been adopted to obtain approximate solutions of the improved Boussinesq equation.

Meshless methods [17] have been rapidly developed in the past thirty years to mitigate the meshing-related issues in classical numerical methods such as the FDM and the FEM. Apart from the absence of elements, another outstanding merit of meshless methods is that, meshless shape functions and then meshless solutions are frequently generated with high accuracy. The moving least square (MLS) approximation is one of the most crucial approach to generate meshless shape functions.[17–21] Some improvements of the MLS, such as the interpolating MLS,[22,23] the complex variable MLS,[24–26] the improved complex variable MLS,[27] the improved interpolating MLS,[28] the complex variable interpolating MLS,[29] the stabilized MLS,[30] and the augmented MLS,[31] have also been proposed to enhance the performance of the MLS.

The improved moving least square (IMLS) approximation[32] is an improved version of the MLS approximation. By using weighted orthogonal basis functions instead of polynomial basis functions, the IMLS produces diagonal system matrices and then possesses a higher computational efficiency than the MLS. Recently, shifted and scaled basis functions have been used to improve the computational stability and precision of the IMLS approximation.[33] Based on the IMLS approximation, meshless methods such as the boundary element-free method,[17,32] the improved element-free Galerkin method,[17,34–36] and the improved Galerkin boundary node method[37] have been proposed and implemented for problems in various fields of physics and engineering.

In this paper, an IMLS meshless method is developed for the numerical solution of the nonlinear improved Boussinesq equation. After the approximation of temporal derivatives, the original time-dependent improved Boussinesq equation is reduced to a set of time-independent equations. Then, the IMLS approximation is used to establish the systems of discrete algebraic equations, where shifted and scaled basis functions are used to guarantee convergence and stability of numerical results. Finally, an iterative algorithm is presented to solve the nonlinear algebraic systems. Numerical experiments involving propagation of single solitary wave and collision of two solitary waves are presented to demonstrate the efficiency of the method. Numerical results reveal that the current IMLS meshless method yields much less error than the FDM, the FEM, the FVEM and the LDG method.

*Project supported by the National Natural Science Foundation of China (Grant No. 11971085), the Fund from the Chongqing Municipal Education Commission, China (Grant Nos. KJZD-M201800501 and CXQT19018), and the Chongqing Research Program of Basic Research and Frontier Technology, China (Grant No. cstc2018jcyjAX0266).

†Corresponding author. E-mail: lxlmath@163.com

© 2021 Chinese Physical Society and IOP Publishing Ltd

2. Problem description

Consider the following nonlinear improved Boussinesq equation:

$$u_{tt} = u_{xx} + u_{xxtt} + \left(u^2\right)_{xx}, \quad x \in \Omega = (a,b), \quad t \in (0,T], \tag{1}$$

with initial conditions

$$u(x,0) = f(x), \quad u_t(x,0) = g(x), \quad x \in \Omega, \tag{2}$$

and boundary conditions

$$u(x,t) = 0, \quad x \in \Gamma = \partial\Omega, \quad t \in (0,T], \tag{3}$$

where the function $u = u(x,t)$ is unknown at position x and time t, the subscript x (or t) denotes differentiation with respect to x (or t), and the functions $f(x)$ and $g(x)$ are known.

The well-known bad Boussinesq equation $u_{tt} = u_{xx} + u_{xxxx} + \left(u^2\right)_{xx}$ is unstable at short wavelengths.[1] By replacing u_{xxxx} with u_{xxtt}, the nonlinear improved Boussinesq equation (1) is physically stable.[1]

3. Approximation of temporal derivatives

According to the Taylor series, the temporal derivatives can be approximated by the difference quotient as[32]

$$u_{tt}(x,k\tau) \approx \frac{u^{k+1}(x) - 2u^k(x) + u^{k-1}(x)}{\tau^2}, \tag{4}$$

$$u_{xxtt}(x,k\tau) \approx \frac{u_{xx}^{k+1}(x) - 2u_{xx}^k(x) + u_{xx}^{k-1}(x)}{\tau^2}, \tag{5}$$

where $\tau > 0$ is the time-step size, and $u^k(x) = u(x,k\tau)$ and $u_{xx}^k(x) = u_{xx}(x,k\tau)$ for $k = 0,1,2,\ldots$

In view of the approximation[6]

$$v(x,k\tau) \approx v^{k+1}(x) - v^k(x) + v^{k-1}(x),$$
$$v = u,\ u_x \text{ or } u_{xx},$$

the nonlinear term $\left(u^2\right)_{xx} = 2\left[uu_{xx} + (u_x)^2\right]$ can be approximated as

$$\begin{aligned}&\left(u^2\right)_{xx}(x,k\tau)\\ \approx\ & 2\left\{\left(u^{k+1} - u^k + u^{k-1}\right)\left(u_{xx}^{k+1} - u_{xx}^k + u_{xx}^{k-1}\right)\right.\\ &\left. + \left(u_x^{k+1} - u_x^k + u_x^{k-1}\right)^2\right\}.\end{aligned} \tag{6}$$

According to Eqs. (4)–(6), equation (1) can be approximated as

$$\begin{aligned}&\left[2\tau^2\left(u^k - u^{k-1}\right) - \tau^2 - 1\right]u_{xx}^{k+1}\\ &+4\tau^2\left(u_x^k - u_x^{k-1}\right)u_x^{k+1} + \left[1 + 2\tau^2\left(u_{xx}^k - u_{xx}^{k-1}\right)\right]u^{k+1}\\ &-2\tau^2\left[u^{k+1}u_{xx}^{k+1} + \left(u_x^{k+1}\right)^2\right]\\ =\ & \left(\tau^2+1\right)u_{xx}^{k-1} - u^{k-1} - \left(\tau^2+2\right)u_{xx}^k + 2u^k\\ &+2\tau^2\left[\left(u^k - u^{k-1}\right)\left(u_{xx}^k - u_{xx}^{k-1}\right) + \left(u_x^k - u_x^{k-1}\right)^2\right],\\ &x \in \Omega, \quad k = 0,1,2,\ldots\end{aligned} \tag{7}$$

In view of Eq. (2), we have

$$u^0(x) = f(x), \quad x \in \Omega. \tag{8}$$

Besides, using the difference quotient formula $u_t(x,0) \approx \left(u^1(x) - u^{-1}(x)\right)/(2\tau)$ yields

$$\begin{aligned}&u^{-1} = u^1 - 2\tau g, \quad u_x^{-1} = u_x^1 - 2\tau g_x,\\ &u_{xx}^{-1} = u_{xx}^1 - 2\tau g_{xx}, \quad x \in \Omega.\end{aligned} \tag{9}$$

Then, letting $k = 0$ in Eq. (7) and using Eqs. (8) and (9), one obtains

$$\begin{aligned}&\left[\tau^2(f + 2\tau g) - 0.5\left(\tau^2+1\right)\right]u_{xx}^1 + 2\tau^2\left(f_x + 2\tau g_x\right)u_x^1\\ &+\left[0.5 + \tau^2\left(f_{xx} + 2\tau g_{xx}\right)\right]u^1 - 2\tau^2\left[u^1u_{xx}^1 + \left(u_x^1\right)^2\right]\\ =\ & 0.5\left[f + \tau g - \left(0.5\tau^2+1\right)f_{xx} - \tau\left(\tau^2+1\right)g_{xx}\right.\\ &\left.+\tau^2(f + 2\tau g)\left(f_{xx} + 2\tau g_{xx}\right) + \tau^2\left(f_x + 2\tau g_x\right)^2\right]\end{aligned} \tag{10}$$

for $x \in \Omega$. Therefore, the time-dependent improved Boussinesq equation (1) is reduced to the time-independent equations (10) for $k = 0$ and (7) for $k = 1,2,\ldots$ with boundary conditions

$$u^{k+1}(x) = 0, \quad x \in \Gamma, \quad k = 0,1,2,\ldots \tag{11}$$

Note that in the case of $k = 1$, we have $u^0 = f$, $u_x^0 = f_x$, and $u_{xx}^0 = f_{xx}$ in Eq. (7).

4. Discretization of spatial derivatives

In the IMLS approximation, the solutions $u^{k+1}(x)$ of Eqs. (7) and (10) can be approximated as

$$\begin{aligned}&u^{k+1}(x) \approx u_h^{k+1}(x) = \sum_{i=1}^{N}\Phi_i(x)\,u_i^{k+1},\\ &x \in \Omega \cup \Gamma, \quad k = 0,1,2,\ldots,\end{aligned} \tag{12}$$

where u_i^{k+1} are approximate values of $u^{k+1}(x_i)$, $\{x_i\}_{i=1}^N$ are N nodes in $\Omega \cup \Gamma = [a,b]$ with $a = x_1 < x_2 < \ldots < x_N = b$ and nodal spacing $h = \max_{1 \le i \le N-1}(x_{i+1} - x_i)$, and

$$\Phi_i(x) = \begin{cases} w_i(x)\sum\limits_{j=1}^{m}\frac{q_j(x_i)q_j(x)}{(q_j,q_j)_x}, & i = I_k \in \Lambda(x),\\ 0, & i \notin \Lambda(x),\end{cases} \quad 1 \le i \le N, \tag{13}$$

where m is the number of the basis, $w_i(x)$ are weight functions. In this paper,

$$w_i(x) = \frac{\exp\left(-(|x - x_i|/h)^2\right) - \exp\left(-(r_i/h)^2\right)}{1 - \exp\left(-(r_i/h)^2\right)},$$

where $r_i = 4.5h$ is the radius of the influence domain of the node x_i. Besides, $\Lambda(x) = \left\{I_1, I_2, \ldots, I_{\tau(x)}\right\}$ is the set of sequence numbers of nodes whose influence domains cover

x, the inner product $(\cdot,\cdot)_x$ is defined for functions v_1 and v_2 as $(v_1,v_2)_x = \sum_{i\in\Lambda(x)} w_i(x)\, v_1(x_i)\, v_2(x_i)$, and $q_j(x)$ are the weighted orthogonal functions,

$$q_1(x)=1,\quad q_i(x)=p_i(x)-\sum_{k=1}^{i-1}\frac{(p_i,q_k)_x}{(q_k,q_k)_x}q_k(x),\quad i=2,3,\ldots m. \tag{14}$$

In the original IMLS approximation, the basis functions $p_i(x)$ in Eq. (14) are usually chosen as the following non-shifted and non-scaled functions[17,32]

$$p_i(x)=x^{i-1},\quad i=2,3,\ldots m. \tag{15}$$

In this case, the stability of the original IMLS approximation deteriorates severely as the nodal spacing h decreases. In the stabilized IMLS approximation, the basis functions $p_i(x)$ are chosen as the following shifted and scaled functions,[30,33]

$$p_i(x)=\left(\frac{x-x^e}{h}\right)^{i-1},\quad i=2,3,\ldots,m, \tag{16}$$

where x^e is a fixed point located on the influence domain of the evaluation point x. Theoretical analysis and numerical verification indicate that the stabilized IMLS approximation can eliminate the instabilities of the original IMLS approximation and thus produces efficient numerical solutions.[30,33]

Differentiating Eq. (12) yields

$$\begin{aligned} u_x^{k+1}(x)&=\sum_{i=1}^{N}\Phi_{i,x}(x)\,u_i^{k+1},\\ u_{xx}^{k+1}(x)&=\sum_{i=1}^{N}\Phi_{i,xx}(x)\,u_i^{k+1},\\ x&\in\Omega\cup\Gamma,\quad k=0,1,2,\ldots \end{aligned} \tag{17}$$

Inserting Eqs. (12) and (17) into Eqs. (7), (10) and (11), collocating Eqs. (7) and (10) for internal nodes $\{x_i\}_{i=2}^{N-1}$, collocating Eq. (11) for boundary nodes x_1 and x_N, we obtain the following nonlinear algebraic systems

$$\boldsymbol{A}^k\boldsymbol{u}^{k+1}-2\tau^2\boldsymbol{f}\left(\boldsymbol{u}^{k+1}\right)=\boldsymbol{b}^k,\quad k=0,1,2,\ldots, \tag{18}$$

where

$$\boldsymbol{u}^{k+1}=\left(u_1^{k+1},u_2^{k+1},\ldots,u_N^{k+1}\right)^{\mathrm{T}},\quad k=0,1,2,\ldots$$

Besides,

$$\begin{aligned}\left[\boldsymbol{f}\left(\boldsymbol{u}^{k+1}\right)\right]_j=&\left[\sum_{i=1}^{N}\Phi_i(x_j)\,u_i^{k+1}\right]\left[\sum_{i=1}^{N}\Phi_{i,xx}(x_j)\,u_i^{k+1}\right]\\&+\left[\sum_{i=1}^{N}\Phi_{i,x}(x_j)\,u_i^{k+1}\right]^2,\quad k=0,1,2,\ldots\end{aligned} \tag{19}$$

for $j=2,3,\ldots,N-1$, while $\left[\boldsymbol{f}\left(\boldsymbol{u}^{k+1}\right)\right]_j=0$ for $j=1,N$ and $k=0,1,2,\ldots$. Moreover,

$$\begin{aligned}[\boldsymbol{A}^k]_{ij}=&\{2\tau^2[u^k(x_j)-u^{k-1}(x_j)]-\tau^2-1\}\Phi_{i,xx}(x_j)\\&+4\tau^2[u_x^k(x_j)-u_x^{k-1}(x_j)]\Phi_{i,x}(x_j)\\&+\{1+2\tau^2[u_{xx}^k(x_j)-u_{xx}^{k-1}(x_j)]\}\Phi_i(x_j),\\&k=1,2,\ldots,\end{aligned} \tag{20}$$

$$\begin{aligned}\left[\boldsymbol{A}^0\right]_{ij}=&\left\{\tau^2[f(x_j)+2\tau g(x_j)]-0.5\left(\tau^2+1\right)\right\}\Phi_{i,xx}(x_j)\\&+2\tau^2\left[f_x(x_j)+2\tau g_x(x_j)\right]\Phi_{i,x}(x_j)\\&+\left\{0.5+\tau^2\left[f_{xx}(x_j)+2\tau g_{xx}(x_j)\right]\right\}\Phi_i(x_j)\end{aligned} \tag{21}$$

for $i=1,2,\ldots,N$ and $j=2,3,\ldots,N-1$, while $\left[\boldsymbol{A}^k\right]_{ij}=\Phi_i(x_j)$ for $i=1,2,\ldots,N$, $j=1,N$ and $k=0,1,2,\ldots$. Furthermore,

$$\begin{aligned}[\boldsymbol{b}^k]_j=&\left(\tau^2+1\right)u_{xx}^{k-1}(x_j)-u^{k-1}(x_j)\\&-\left(\tau^2+2\right)u_{xx}^k(x_j)+2u^k(x_j)\\&+2\tau^2\left\{[u^k(x_j)-u^{k-1}(x_j)][u_{xx}^k(x_j)-u_{xx}^{k-1}(x_j)]\right.\\&\left.+[u_x^k(x_j)-u_x^{k-1}(x_j)]^2\right\},\quad k=1,2,\ldots\end{aligned} \tag{22}$$

$$\begin{aligned}\left[\boldsymbol{b}^0\right]_j=&\,0.5\left\{f(x_j)+\tau g(x_j)\right.\\&-\left(0.5\tau^2+1\right)f_{xx}(x_j)-\tau\left(\tau^2+1\right)g_{xx}(x_j)\\&+\tau^2[f(x_j)+2\tau g(x_j)][f_{xx}(x_j)+2\tau g_{xx}(x_j)]\\&\left.+\tau^2[f_x(x_j)+2\tau g_x(x_j)]^2\right\},\end{aligned} \tag{23}$$

for $j=2,3,\ldots,N-1$, while $\left[\boldsymbol{b}^k\right]_j=0$ for $j=1,N$ and $k=0,1,2,\ldots$.

5. Algorithms

In view of Eq. (19), the algebraic systems given in Eq. (18) are nonlinear. The following iterative algorithm is adopted to solve these nonlinear systems.

Algorithm 1 Set $l=0$ and $\boldsymbol{u}^{k+1,l}=\boldsymbol{u}^k$, and choose a tolerance $\varepsilon>0$.

1. Linearize Eq. (18) as

$$\boldsymbol{A}\boldsymbol{u}^{k+1,l+1}=2\tau^2\boldsymbol{f}\left(\boldsymbol{u}^{k+1,l}\right)+\boldsymbol{b}^k. \tag{24}$$

2. Obtain $\boldsymbol{u}^{k+1,l+1}$ by solving Eq. (24).

3. Update l to $l+1$ and go to (a) if $\left\|\boldsymbol{u}^{k+1,l+1}-\boldsymbol{u}^{k+1,l}\right\|/\left\|\boldsymbol{u}^{k+1,l+1}\right\|>\varepsilon$. Otherwise, stop the algorithm and output $\boldsymbol{u}^{k+1}=\boldsymbol{u}^{k+1,l+1}$.

In this paper, the Matlab function $\boldsymbol{u}^{k+1,l+1}=\boldsymbol{A}^{k+1,l+1}\backslash\left(2\tau^2\boldsymbol{f}\left(\boldsymbol{u}^{k+1,l}\right)+\boldsymbol{b}^k\right)$ is used to solve the linear system given in Eq. (24).

Theorem 1 Let

$$[\bar{A}]_{ij}=\begin{cases}-\Phi_{i,xx}(x_j)+\Phi_i(x_j), & j=2,3,\ldots,N-1,\\ \Phi_i(x_j), & j=1,N,\end{cases}\qquad i=1,2,\ldots,N. \tag{25}$$

If $\bar{\boldsymbol{A}}^{-1}$ exists and $\tau h < \delta$ for a positive constant δ, then $\lim_{l\to\infty} \boldsymbol{u}^{(k+1),l} = \boldsymbol{u}^{(k+1)}$.

Proof According to Eq. (24), we have

$$\boldsymbol{A}\boldsymbol{u}^{k+1,l+2} = 2\tau^2 \boldsymbol{f}\left(\boldsymbol{u}^{k+1,l+1}\right) + \boldsymbol{b}^k. \tag{26}$$

Then, subtracting Eq. (24) from Eq. (26) obtains

$$\begin{aligned}&\boldsymbol{u}^{k+1,l+2} - \boldsymbol{u}^{k+1,l+1}\\ &= 2\tau^2 \boldsymbol{A}^{-1}\left[\boldsymbol{f}\left(\boldsymbol{u}^{k+1,l+1}\right) - 2\tau^2 \boldsymbol{f}\left(\boldsymbol{u}^{k+1,l}\right)\right].\end{aligned}$$

Hence,

$$\begin{aligned}&\left\|\boldsymbol{u}^{k+1,l+2} - \boldsymbol{u}^{k+1,l+1}\right\|_\infty\\ &\le 2\tau^2 \left\|\boldsymbol{A}^{-1}\right\|_\infty \left\|\boldsymbol{f}\left(\boldsymbol{u}^{k+1,l+1}\right) - \boldsymbol{f}\left(\boldsymbol{u}^{k+1,l}\right)\right\|_\infty.\end{aligned} \tag{27}$$

On the one hand, equations (20) and (25) show that $\lim_{\tau\to 0} \boldsymbol{A} = \bar{\boldsymbol{A}}$. In view of the existence of $\bar{\boldsymbol{A}}^{-1}$, for τ sufficiently small, there is a positive constant $\mathcal{C}_{\boldsymbol{A}}$ such that

$$\left\|\boldsymbol{A}^{-1}\right\|_\infty \le \mathcal{C}_{\boldsymbol{A}}. \tag{28}$$

On the other hand, according to Ref. [30], there is a constant $\mathcal{C}_{\Phi}$ independent of h such that $\left\|\mathrm{d}^\lambda \Phi_i(x)/\mathrm{d}x^\lambda\right\|_\infty \le \mathcal{C}_{\Phi} h^\lambda$. Thus, using to Eq. (19) yields

$$\begin{aligned}&\left\|\boldsymbol{f}\left(\boldsymbol{u}^{k+1,l+1}\right) - \boldsymbol{f}\left(\boldsymbol{u}^{k+1,l}\right)\right\|_\infty\\ &\le \mathcal{C}_{\Phi} h^2 \left\|\boldsymbol{u}^{k+1,l+1} - \boldsymbol{u}^{k+1,l}\right\|_\infty.\end{aligned} \tag{29}$$

Substituting Eqs. (28) and (29) into Eq. (27), we have

$$\begin{aligned}&\left\|\boldsymbol{u}^{k+1,l+2} - \boldsymbol{u}^{k+1,l+1}\right\|_\infty\\ &\le 2\tau^2 \mathcal{C}_{\boldsymbol{A}} \mathcal{C}_{\Phi} h^2 \left\|\boldsymbol{u}^{k+1,l+1} - \boldsymbol{u}^{k+1,l}\right\|_\infty.\end{aligned}$$

Let $\delta = 1/\sqrt{2\mathcal{C}_{\boldsymbol{A}}\mathcal{C}_{\Phi}} > 0$. Then, when $\tau h < \delta$, we have the following error reduction relation

$$\left\|\boldsymbol{u}^{k+1,l+2} - \boldsymbol{u}^{k+1,l+1}\right\|_\infty < \left\|\boldsymbol{u}^{k+1,l+1} - \boldsymbol{u}^{k+1,l}\right\|_\infty,$$

which implies $\lim_{l\to\infty} \left\|\boldsymbol{u}^{k+1,l+1} - \boldsymbol{u}^{k+1,l}\right\|_\infty = 0$. Consequently, we obtain $\lim_{l\to\infty} \boldsymbol{u}^{k+1,l} = \mathrm{u}^{k+1}$.

To sum up, the algorithm of the IMLS approximation for the nonlinear improved Boussinesq equation given in Eqs. (1)–(3) follows.

Algorithm 2 Choose the time step size τ, the desirable time T, and N nodes $\{x_i\}_{i=1}^N$ in $\Omega \cup \Gamma$.

1. Compute shape functions using Eq. (13).

2. Set $k = 0$. Assemble the matrix $\boldsymbol{A}^0$ and vectors $\boldsymbol{f}\left(\boldsymbol{u}^1\right)$ and $\boldsymbol{b}^0$ using Eqs. (21), (19), and (23), respectively. Solve the nonlinear system (18) using Algorithm 1 for $k = 0$ to obtain $\boldsymbol{u}^1$.

3. Update k to $k+1$. Compute $u^k(x_j)$, $u_x^k(x_j)$, and $u_{xx}^k(x_j)$ using Eqs. (12) and (17), respectively. Assemble the matrix $\boldsymbol{A}^k$ and vectors $\boldsymbol{f}\left(\boldsymbol{u}^{k+1}\right)$ and $\boldsymbol{b}^k$ using Eqs. (20), (19), and (22), respectively. Solve the nonlinear system (17) using Algorithm 1 to obtain $\boldsymbol{u}^{k+1}$. Repeat this step until $(k+1)\tau = T$.

4. Compute the numerical solution of the improved Boussinesq equation using Eq. (12).

6. Numerical results

6.1. Propagation of single solitary wave

Consider the improved Boussinesq equation (1) with the initial conditions

$$\begin{aligned}u(x,0) &= A\mathrm{sech}^2\left(\sqrt{\frac{A}{6}}\frac{x-x_0}{c}\right), \quad x\in(a,b),\\ u_t(x,0) &= 2A\sqrt{\frac{A}{6}}\mathrm{sech}^2\left(\sqrt{\frac{A}{6}}\frac{x-x_0}{c}\right)\\ &\quad\times\tanh\left(\sqrt{\frac{A}{6}}\frac{x-x_0}{c}\right), \quad x\in(a,b),\end{aligned}$$

where A, $x_0 = 0$, and $c = \sqrt{1+2A/3}$ are the amplitude, initial location, and wave velocity, respectively. This example has a single solitary wave analytical solution,

$$u(x,t) = A\mathrm{sech}^2\left(\sqrt{\frac{A}{6}}\frac{x-x_0-ct}{c}\right), \quad x\in(a,b), \quad t>0.$$

The propagation of the single solitary wave and the associated error $|u-u_h|$ for $x\in[-80,140]$ and $t\in[0,72]$ are presented in Fig. 1, while the results at $t = 72$ are presented in Fig. 2. In this analysis, we use the time-step size $\tau = 0.001$, the nodal spacing $h = 0.1$, and various amplitudes $A = 0.25$, 0.5, 0.75, and 0.9. It can be observed from these figures that the single solitary wave propagates with no change in form, and the current IMLS method obtains very accurate numerical results.

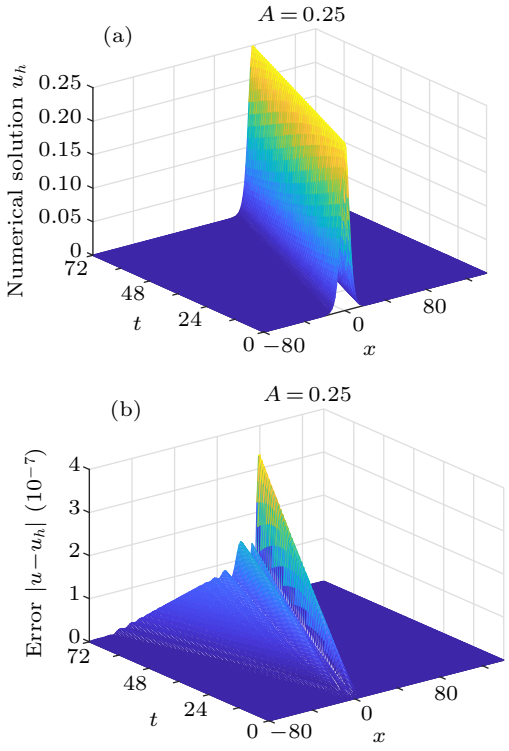


Fig. 1. Results of (a) the numerical solution and (b) the associated error obtained using $h = 0.1$ and $\tau = 0.001$ for $x\in[-80,140]$ and $t\in[0,72]$.

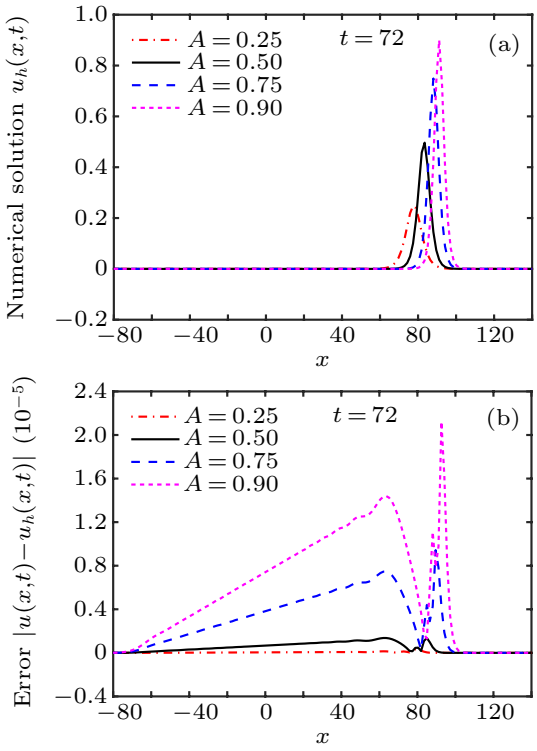


Fig. 2. Results of (a) the numerical solution u_h and (b) the associated error $|u-u_h|$ obtained using $h=0.1$ and $\tau=0.001$ at $t=72$.

Figure 3 gives the $L_\infty=\max_{1\le i\le N}|u(x_i)-u_h(x_i)|$ error of the IMLS, FDM,[7] FEM,[6] and FVEM[12] for various amplitudes $A=0.25$, 0.5, 0.75, and 0.9 obtained using $h=0.1$ and $\tau=0.001$ for $x\in[-80,140]$ and $t\in[0,72]$, figure 4 gives the

$$L_2=\sqrt{h\sum_{i=1}^{N}[u(x_i)-u_h(x_i)]^2}$$

and L_∞ errors of the IMLS and LDG[15] for $A=0.5$, $x\in[-100,100]$, and $t\in[0,1]$, while figure 5 gives the L_2 and L_∞ errors of the IMLS, FVEM1,[11] and FVEM2[12] for $A=0.5$, $x\in[-60,100]$, and $t\in[0,1]$. It can be found from Figs. 3–5 that the current IMLS method produces much less error than the other methods.

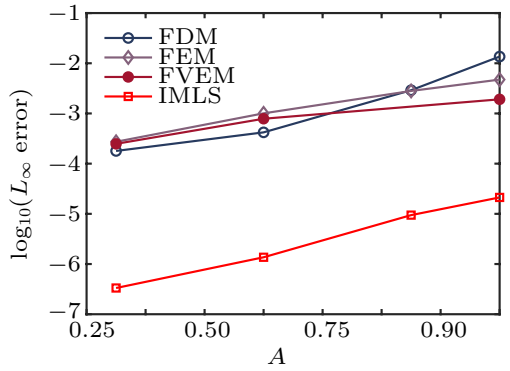


Fig. 3. Comparison of the L_∞ error for FDM,[7] FEM,[6] FVEM,[12] and IMLS.

Figures 6 and 7 show the convergence of the current IMLS method in time and space, respectively. In this analysis, we use $x\in[-60,100]$, $t\in[0,1]$, and various amplitudes $A=0.25$, 0.5, 0.75, and 0.9. Obviously, both the L_2 and L_∞ errors of the IMLS method decrease rapidly as the time-step size τ and the nodal spacing h decrease, and the experimental convergence forms are about $\mathrm{O}(\tau^2)$ and $\mathrm{O}(h^4)$. Thus, the current IMLS method owns very good convergence properties in both time and space.

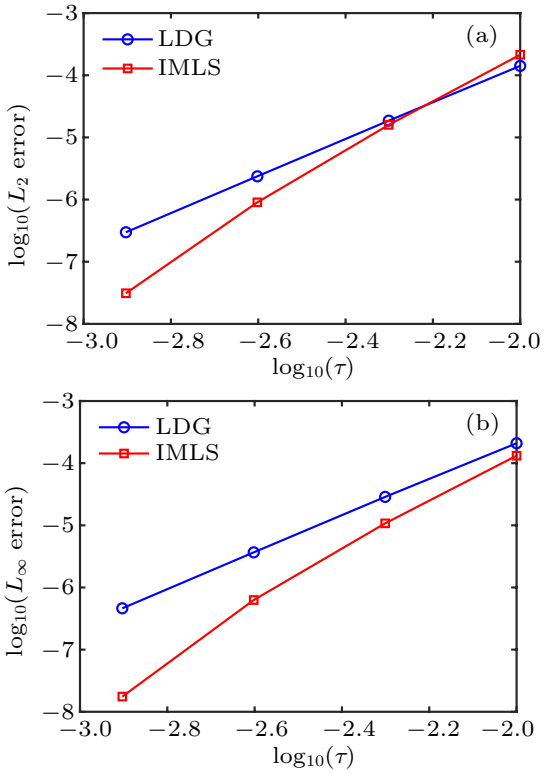


Fig. 4. The comparison of (a) L_2 and (b) L_∞ errors for the LDG[15] and IMLS.

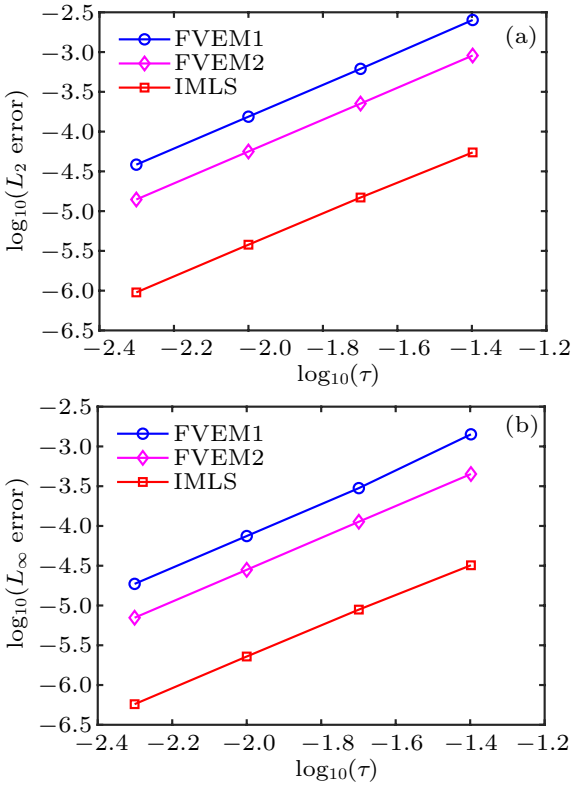


Fig. 5. The comparison of (a) L_2 and (b) L_∞ errors for FVEM1,[11] FVEM2,[12] and IMLS.

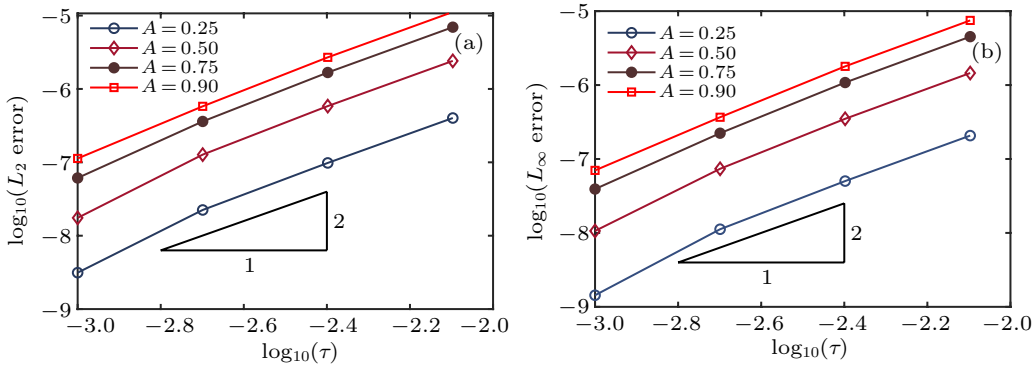


Fig. 6. Convergence of the IMLS method with respect to the time-step size τ obtained using $h = 0.1$: (a) L_2 and (b) L_∞ errors.

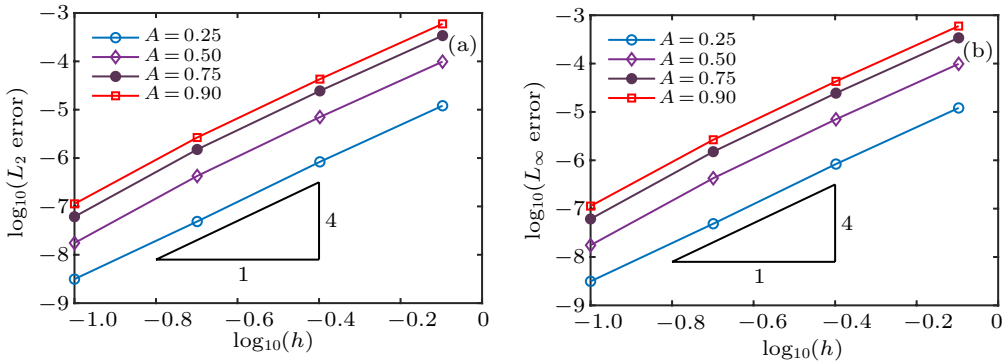


Fig. 7. Convergence of the IMLS method with respect to the nodal spacing h obtained using $\tau = 0.001$: (a) L_2 and (b) L_∞ errors.

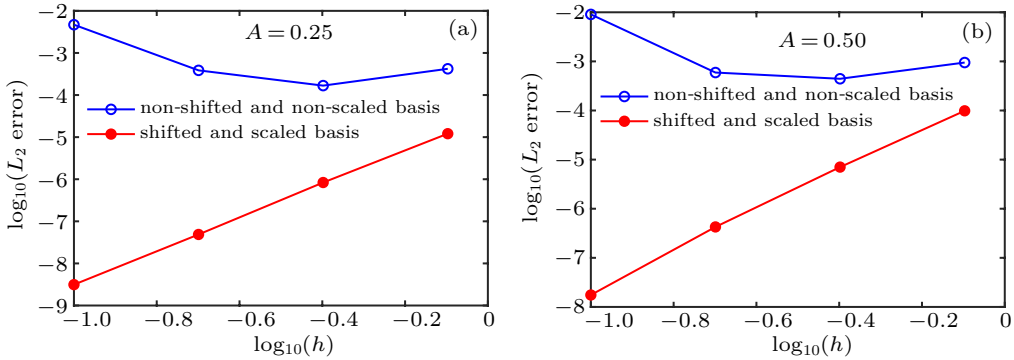


Fig. 8. Convergence and stability of the IMLS method using two kinds of basis functions.

In the original IMLS method, the non-shifted and non-scaled basis functions given in Eq. (15) are used to form shape functions. While in the current IMLS method, the shifted and scaled basis functions given in Eq. (16) are used to form shape functions. Convergence and stability of the IMLS method based on the two kinds of basis functions are shown in Fig. 8. In this analysis, we use $x \in [-60, 100]$, $t \in [0, 1]$, $\tau = 0.001$, and $A = 0.25$ and 0.5. It can be found that the numerical results obtained by the non-shifted and non-scaled basis are instability and not convergent, while the results obtained by the shifted and scaled basis converge rapidly and monotonously. Therefore, the shifted and scaled basis produces lower computational error and has better numerical convergence and stability than the non-shifted and non-scaled basis.

6.2. Collision of two solitary waves

Consider the improved Boussinesq equation (1) with the initial conditions

$$u(x,0) = \sum_{i=1}^{2} A_i \operatorname{sech}^2\left(\sqrt{\frac{A_i}{6}}\frac{x-x_{0i}}{c_i}\right), \quad x \in (-80, 100),$$

$$u_t(x,0) = 2\sum_{i=1}^{2} A_i\sqrt{\frac{A_i}{6}}\operatorname{sech}^2\left(\sqrt{\frac{A_i}{6}}\frac{x-x_{0i}}{c_i}\right) \times \tanh\left(\sqrt{\frac{A_i}{6}}\frac{x-x_{0_i}}{c_i}\right), \quad x \in (-80, 100),$$

where A_1 and A_2 are the amplitudes of the two solitary waves, $x_{01} = -20$ and $x_{02} = 30$ are the initial locations of the two waves, and $c_1 = \sqrt{1+2A_1/3}$ and $c_2 = -\sqrt{1+2A_2/3}$ are the wave velocities.

Figure 9 gives the evolution of the two solitary waves

for equal amplitudes $A_1 = A_2 = 0.4$ and $A_1 = A_2 = 2.0$, figure 10 gives the evolution for unequal amplitudes $A_1 = 0.4$ and $A_2 = 0.5$, 1.5 and 2.5, while figure 11 gives the numerical solutions for various amplitudes at $t = 60$. In this analysis, we use the time-step size $\tau = 0.001$ and the nodal spacing $h = 0.1$.

We can see from Figs. 9 and 10 that the two waves begin to move independently, then collide gradually, and finally pass through each other. At the collision time, the two waves almost disappear, but after a while, they appear and regain their amplitudes, shapes and speeds. Besides, figures 9(a), 10(a), and 11(a) show that there are invisible secondary waves after the collision and thus the collision is elastic in the case of $A_1 = A_2 = 0.4$, and the case of $A_1 = 0.4$ and $A_2 = 0.5$. However, figures 9(b), 10(b), 10(c), and 11(b) show that there are visible secondary waves after the collision and thus the collision is inelastic in the case of $A_1 = A_2 = 2.0$, and the two cases of $A_1 = 0.4$ and $A_2 = 1.5$ and 2.5. Moreover, the larger amplitudes are, the stronger secondary waves are. Thus, the collision and the inelasticity rely on the amplitudes of the two solitary waves.

These results are in good agreement with those obtained by FDM,[7–9] FEM,[10] FVEM,[11,12] Fourier pseudospectral method,[13] radial basis functions method,[14] and LDG method.[15]

To show the collision quantitatively, Table 1 gives the values of the inelasticity coefficient $K = A_m/\max(A_1, A_2)$ obtained by the current IMLS method, FDM,[7] FVEM,[12] and LDG.[15] Here, A_m is the maximum joint amplitude at the collision time. It can be found that the IMLS values are similar as those in Refs. [7,12,15].

Table 1. The inelasticity coefficient K for various amplitudes.

A_1	A_2	IMLS	FDM	FVEM	LDG
0.4	0.4	1.80502	1.79105	1.80709	1.80607
2.0	2.0	1.65644	1.6294	1.66043	1.65809
0.4	0.5	1.61569	1.59228	1.61788	1.61692
0.4	1.5	1.14492	1.08353	1.14648	1.14507
0.4	2.5	1.06728	1.02672	1.06914	1.06752

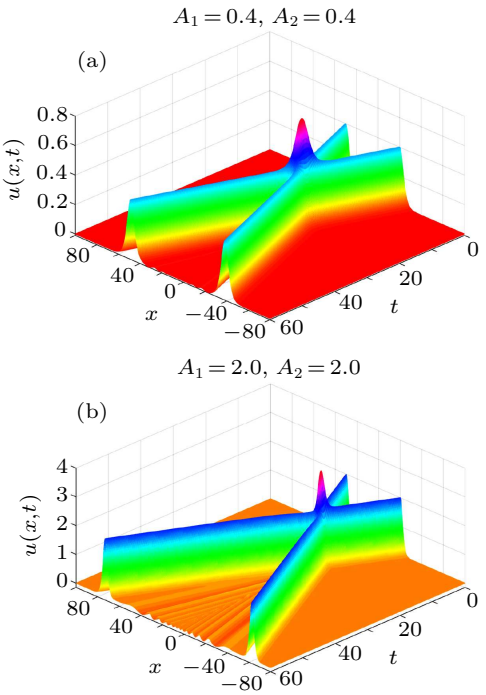


Fig. 9. Collision of two solitary waves for (a) $A_1 = A_2 = 0.4$ and (b) $A_1 = A_2 = 2.0$.

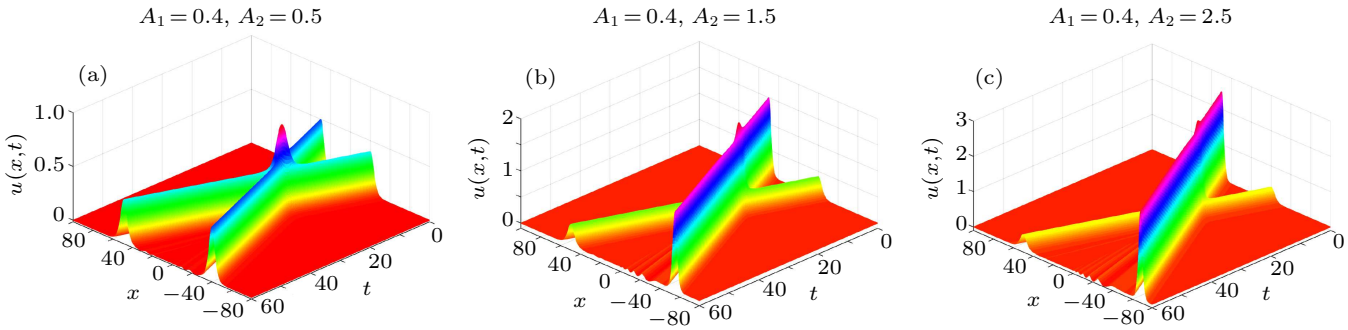


Fig. 10. Collision of two solitary waves for (a) $A_1 = 0.4$ and $A_2 = 0.5$, (b) $A_1 = 0.4$ and $A_2 = 1.5$, and (c) $A_1 = 0.4$ and $A_2 = 2.5$.

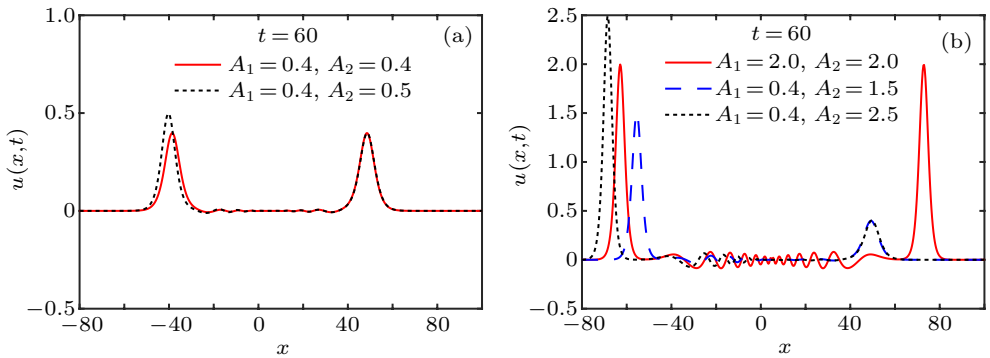


Fig. 11. Results of the solutions for various amplitudes at $t = 60$.

7. Conclusions

An IMLS meshless method is developed in this paper for the numerical analysis of the nonlinear improved Boussinesq equation. To illustrate the accuracy, convergence and efficiency of the method, numerical experiments involving propagation of single solitary wave and collision of two solitary waves are presented. Computational errors are compared with those obtained by FDM, FEM, FVEM, and LDG methods. These comparisons reveal that the current IMLS method yields much less errors. Besides, numerical results indicate that the errors of the IMLS method decrease rapidly as the time-step size and the nodal spacing decrease, and the method owns very good convergence properties with the second-order accuracy in time and the fourth-order accuracy in space. Moreover, the shifted and scaled basis functions produce lower error and have better numerical convergence and stability than the previously non-shifted and non-scaled basis functions. Future investigations can consider the performance of IMLS method for other nonlinear partial differential equations such as the unsteady Schrödinger equation,[35] Camassa and Holm equation,[36] Kadomtsev–Petviashvili equation,[39] and Euler equation.[40]

References

[1] Bogolubsky I L 1997 *Comput. Phys. Commun.* **13** 149
[2] Wazwaz A M 2009 *Partial Differential Equations and Solitary Waves Theory* (Berlin: Springer)
[3] Zhang T, Lin Z H, Huang G Y, Fan C M and Li P W 2020 *Ocean Eng.* **198** 106957
[4] Soerensen M P, Christiansen P L and Lomdahl P S 1984 *J. Acoust. Soc. Am.* **76** 871
[5] Berezin Y A and Karpman V I 1967 *J. Exp. Theoret. Phys.* **24** 1049
[6] Irk D and Dağ İ 2010 *Numer. Methods Part. Differ. Equ.* **26** 1316
[7] Bratsos A G 2009 *Chaos, Solitons and Fractals* **40** 2083
[8] Lu F Q, Song Z Y and Zhang Z 2016 *J. Comput. Math.* **34** 462
[9] Wongsaijai B, Oonariya C and Poochinapan K 2020 *Math. Comput. Simulation* **178** 125
[10] Karaagac B, Ucar Y and Esen A 2018 *Filomat* **32** 5573
[11] Wang Q X, Zhang Z Y, Zhang X H and Zhu Q Y 2014 *J. Comput. Phys.* **270** 58
[12] Yan J L, Deng D W, Lu F Q and Zhang Z Y 2020 *Appl. Math. Model.* **87** 20
[13] Yan J L, Zhang Z Y, Zhao T J and Liang D 2018 *Numer. Methods Part. Differ. Equ.* **34** 1145
[14] Shokri A and Dehghan M 2010 *Comput. Phys. Commun.* **181** 1990
[15] Li X L, Sun W Z, Xing Y L and Chou C S 2020 *J. Comput. Phys.* **401** 109002
[16] Cai J X, Qin Z L and Bai C Z 2013 *Chin. Phys. Lett.* **30** 070202
[17] Cheng Y M 2015 *Meshless Methods* (Beijing: Science Press) (in Chinese)
[18] Li X L 2016 *Appl. Numer. Math.* **99** 77
[19] Li X L and Dong H Y 2020 *Appl. Math. Comput.* **382** 125326
[20] Li X L and Li S L 2020 *Comput. Math. Appl.* **79** 3297
[21] Zhang T and Li X L 2020 *Appl. Math. Comput.* **380** 125306
[22] Ren H P, Cheng Y M and Zhang W 2010 *Sci. China: Phys. Mech. Astron.* **53** 758
[23] Zhang T and Li X L 2020 *Comput. Math. Appl.* **79** 363
[24] Cheng Y M, Peng M J and Li J H 2005 *Chin. J. Theoret. Appl. Mech.* **37** 719
[25] Li X L 2018 *Appl. Math. Model.* **63** 148
[26] Chen L C and Li X L 2020 *Appl. Math. LeTt.* **101** 106067
[27] Li D M, Bai F N, Cheng Y M and Liew K M 2012 *Comput. Methods Appl. Mech. Eng.* **233** 1
[28] Wang J F, Sun F X and Cheng Y M. 2012 *Chin. Phys. B* **21** 090204
[29] Deng Y J, Liu C, Peng M J and Cheng Y M 2015 *Int. J. Appl. Mech.* **7** 1550017
[30] Li X L and Li S L 2016 *Comput. Math. Appl.* **72** 1515
[31] Qu W Z, Fan C M and Li X L 2020 *Comput. Math. Appl.* **83** 13
[32] Cheng Y M and Peng M J 2005 *Sci. China Ser. G* **48** 641
[33] Tang Y Z and Li X L 2017 *Chin. Phys. B* **26** 030203
[34] Zhang Z, Wang J F, Cheng Y M and Liew K M 2013 *Sci. China: Phys. Mech. Astron.* **56** 1568
[35] Cheng R J and Cheng Y M 2016 *Chin. Phys. B* **25** 020203
[36] Cheng R J and Wei Q 2013 *Chin. Phys. B* **22** 060209
[37] Li X L and Zhang S G 2016 *Appl. Math. Model.* **40** 2875
[38] Burden R L and Faires J D 2011 *Numerical Analysis* (Boston: Cengage Learning)
[39] Cheng X P, Ma W X and Yang Y Q 2019 *Chin. Phys. B* **28** 100203
[40] Qin J X, Chen Y M and Deng X G 2019 *Chin. Phys. B* **28** 104701